

Hotspot and NDVI Differencing Synergy (HANDS): A New Technique for Burned Area Mapping over Boreal Forest

R. H. Fraser,^{*} Z. Li,[†] and J. Cihlar[†]

*B*iomass burning releases significant amounts of trace gases and smoke aerosol into the atmosphere. This has an impact on the Earth's radiation budget, the magnitude of which has not yet been well quantified. Satellite remote sensing is well suited to assessing the area of biomass burning, a prerequisite for estimating emissions at regional and global scales. Commonly used satellite-based techniques for measuring burned areas include thermal hotspot detection and multitemporal NDVI analysis, each having several limitations. Here we present a new, hybrid approach for boreal burned area mapping called HANDS, or hotspot and NDVI differencing synergy. The automated technique was tested using satellite data covering Canada for the 1995 and 1996 fire seasons, and comparing results with official burned area statistics and conventional fire surveys. HANDS computed a national burned forest area of 6.8 million ha in 1995 and 2.0 million ha in 1996, corresponding favorably to Canadian Forest Service estimates of 7.1 million ha and 1.9 million ha, respectively. Moreover, in most cases, the technique accurately delineated the boundaries of individual burns and identified some burns that were missed with conventional mapping. When employed in conjunction with NOAA-AVHRR imagery, HANDS provides a consistent means of mapping large burns (>10 km²), which are characteristic for the boreal forest. New generation sensors (e.g., SPOT VEGETATION, Terra MODIS) should enable its successful application to a wider range of environments. ©Elsevier Science Inc., 2000

INTRODUCTION

Biomass burning causes a wide range of global environmental impacts (Levine, 1996). Most significantly, vegetation fires emit substantial amounts of trace gases (CO₂, CO, CH₄, NO_x) and particulates into the atmosphere (Andreae et al., 1996). Together, these emissions influence the Earth's atmospheric chemistry, radiation budget, and overall climate (Crutzen and Andreae, 1990). The net effect of smoke aerosol on the Earth's radiation budget has not been well quantified, representing a major source of uncertainty in global climate modelling. Biomass burning also has several ecological effects, such as the loss of animal habitat and biodiversity (Lovejoy, 1991), modifying vegetation successional patterns (Christensen, 1993), and altering biological nutrient cycling (Menaut et al., 1993). In order to assess this array of impacts, techniques must be developed for accurately measuring the spatial and temporal distribution of vegetation fires at a global scale.

Due to the ephemeral nature of biomass burning and its wide geographic extent, satellite remote sensing provides the only practical means of monitoring fire distribution. In particular, satellite-based observations offer the potential to accurately quantify the area of vegetation burning. Such information is required to estimate total biomass burning and resulting atmospheric emissions (Setzer and Pereira, 1991; Kasischke et al., 1995). To this end, generally applicable techniques are required to: 1) provide unbiased estimates of burned area; 2) be readily adaptable to a range of input data sets and environmental conditions, without relying on fixed thresholds; and 3) be automated, requiring minimal analyst intervention.

Current satellite-based strategies for large-area burn assessment may be grouped into two categories, active fires (hotspot) detection and postfire burn detection. In hotspot detection, fire thermal energy is used to identify

^{*} Intermap Technologies, Ottawa, Ontario, Canada

[†] Canada Centre for Remote Sensing, Ottawa, Ontario, Canada

Address correspondence to R. Fraser, CCRS, 588 Booth St., Ottawa, ON, Canada K1A 0Y7. E-mail: rfraser@ccrs.nrcan.gc.ca

Received 19 February 1999; revised 15 December 1999.

active fires. The mid-infrared channel (3.55–3.93 μm) of the NOAA Advanced Very High Resolution Radiometer (AVHRR) sensor is most commonly used for this purpose (Flannigan and Vonder Haar, 1986; Kaufman et al., 1990; Setzer and Pereira, 1991; Justice et al., 1996; Li et al., 1997, 1999a; Randriambelo et al., 1998). AVHRR Channel 3 is highly sensitive to targets with thermal emissions in the range for vegetation fires; it may show a large response from a fire covering only a fraction of its nominal 1.2 km² footprint (Robinson, 1991). AVHRR-based hotspot algorithms typically use additional information from other channels to reduce false hotspots caused by highly reflective objects such as cloud, warm surfaces such as bare soil, or sun-glint over water. While channel thresholds are normally optimized for specific regions, some recent algorithms derive them dynamically using contextual information from background pixels (Flasse and Ceccato, 1996; Harris, 1996; Justice et al., 1996). Such algorithms are adaptable to different environments and thus more widely applicable. A contextual algorithm has recently been applied globally as part of the International Geosphere Biosphere Programme, Data and Information Systems (IGBP-DIS) project (IGBP-DIS, 1997; Dwyer et al., 1998).

A primary limitation in assessing burned area by compositing AVHRR hotspots over a given period is that hotspots represent only a series of snapshots of burn activity. Many active fires may be missed due to cloud and limited satellite diurnal sampling (Pereira and Setzer, 1996; Li et al., 1999a). For example, Li et al. (1999a) found that hotspot detection underestimated Canada-wide burned area by 37% in 1994 and 31% in 1995 compared to Canadian Forest Service (CFS) estimates. Conversely, hotspot detection may overestimate burned area if thresholds are applied to environments different from those for which they were derived (Kennedy et al., 1994; Li et al., 1999b). Overestimation may also occur if there is a large proportion of small, subpixel fires that may cause saturation of Channel 3 (Kennedy et al., 1994; Pereira and Setzer, 1996; Randriambelo et al., 1998).

The second family of techniques for burned area assessment detects vegetation damage following fire. For example, Cahoon et al. (1994) applied unsupervised minimum distance classification to AVHRR imagery to identify 14 million ha of east-Asian boreal forest that burned in 1987. Postfire mapping may also be accomplished through multitemporal analysis of a vegetation index. The normalized difference vegetation index (NDVI), providing a measure of vegetation greenness and photosynthetic activity (Running et al., 1986), has most commonly been used for this purpose, although more suitable indices have recently been proposed (Barbosa et al., 1999; Pereira, 1999). NDVI is calculated using AVHRR imagery as in Eq. (1):

$$\text{NDVI} = (\text{Ch2} - \text{Ch1}) / (\text{Ch2} + \text{Ch1}), \quad (1)$$

where Ch1=Channel 1 red reflectance (0.58–0.68 μm) and Ch2=Channel 2 near-infrared reflectance (0.73–1.1 μm). When green vegetation is burned, NDVI decreases owing to a rise in Ch1 reflectance and decrease in Ch2 reflectance. Most fire studies measure the degree of NDVI change by subtracting pre- and postfire NDVI composites (Kasischke et al., 1993; Kasischke and French, 1995; Martin and Chuvieco, 1995; Li et al., 1999b), although NDVI regression (Fernandez et al., 1997) and examination of NDVI time trajectories (Li et al., 1997) have also been found effective. After the NDVI difference is calculated, a suitable threshold is established to separate burned pixels.

A significant advantage of postfire mapping is that, unlike hotspot detection, the indicator of fire remains detectable for a longer period. NDVI differencing is therefore capable of mapping burned areas that may be missed using the hotspot technique. The main drawback of NDVI differencing for burn assessment is the tendency for commission error caused by NDVI decrease unrelated to fire (Kasischke and French, 1995; Li et al., 1999b; this study). Decreases may be attributable to other factors such as drought, seasonal vegetation senescence, timber harvesting, image misregistration, and cloud contamination in the postfire composite. A further difficulty with differencing is that an effective threshold for separating burns is spatially and temporally variable (Kasischke and French, 1995; Fernandez et al., 1997). To compensate for this variation, Fernandez et al. (1997) derived a dynamic threshold based on the magnitude of each pixel's NDVI decrease relative to the NDVI difference variability within the 100×100 km region surrounding each fire. More recently, Roy et al. (1999) developed a multitemporal scar detection algorithm that computes a burn scar index change map. Variable thresholds derived from a hotspot algorithm are then used to classify the change map.

The purpose of this article is to present a new method for burned area mapping that synergistically combines the hotspot and NDVI differencing strategies. The technique, abbreviated HANDS (hotspot and NDVI differencing synergy), uses the strengths of each method to compensate for the limitations of the other. To evaluate its performance, we applied HANDS to mapping forest fire burns across Canada in 1995 and 1996. Results were validated using Canadian Forest Service fire statistics and province-wide burn surveys.

DATA SOURCES

Satellite Data

Three types of input data are required for the HANDS technique: 1) a binary mask of hotspots detected during the period of interest; 2) post- and prefire vegetation index (e.g., NDVI) composites for the period of interest;

and 3) a vegetation mask. In our application of the algorithm to Canada, these data sets were derived from 1.1-km resolution AVHRR imagery from NOAA-11 (1994) and NOAA-14 (post-1994). The processing steps required to produce them are described below.

AVHRR data (High Resolution Picture Transmission format) are received at the Prince Albert receiving station in Saskatchewan and then processed using the high-throughput geocoding and compositing system (GEOCOMP; Robertson et al., 1992). GEOCOMP performs time-dependent calibration of Channels 1 and 2 and correction of Channels 3–5 using onboard calibration information from NOAA. Single-date composites covering the Canadian landmass are registered to Lambert conformal conic projection using an orbit model and ground control points, typically yielding a positional accuracy better than 1 km. Daily images are then composited over 10-day periods using the maximum NDVI criterion. It should be noted that other compositing criteria, such as minimum albedo, have been shown to more effectively retain the burn signal in environments where the spectral response to burning is short-lived, such as savannah (Barbosa et al., 1998). The reason for this is that maximum NDVI will be biased towards selecting pixels from a compositing period that precede burning. Alternatively, when a fire occurs prior to the first cloud-free pixel in a compositing period, maximum NDVI will preferentially select the latest cloud-free data from that period when the burn signal has attenuated. For annual analysis of burned boreal forest, the choice of compositing criterion will be less important since almost all burning has occurred before the postfire composite, while the burn signal continues to remain strong throughout the compositing period.

Further processing of 10-day composites is carried out at Canada Centre for Remote Sensing using the ABC3 methodology (atmospheric, bidirectional, and cloud contamination corrections of CCRS) (Cihlar et al., 1997). For Channels 1 and 2, ABC3 computes top-of-atmosphere reflectance, performs atmospheric corrections, and also corrects for bidirectional reflectance effects. Pixels contaminated by clouds are detected and replaced by linearly interpolating the seasonal trajectory of each channel for that pixel (Cihlar, 1996). Finally, the NDVI is calculated from corrected reflectances, and smoothed in the temporal dimension to obtain a value for each pixel every 10 days during the growing season.

Li et al. (1999a, b) developed a hotspot algorithm for boreal forests that uses the calibrated and georeferenced daily composites from GEOCOMP. The algorithm, dubbed CFDA (Canadian Fire Detection Algorithm), involves marking potential fires using a Channel 3 threshold, then removing false fires using a series of spectral and spatial tests. Annual fire masks were produced for 1994–1997 by summing hotspots detected daily during the April–October forest fire season (Li et al., 1999a).

The HANDS algorithm requires pre- and postfire

vegetation index composites for the period of interest. Recent investigations by Pereira (1999) and Barbosa et al. (1999) demonstrated that AVHRR indices based on the NIR/MIR spectral domain (e.g., GEMI3) provide optimal discrimination of burns in Mediterranean and African environments. Although these studies found that the NDVI was significantly less effective for this purpose, NDVI has been shown to exhibit strong contrast for burned boreal forest during the year in which fire occurs (Kasischke and French, 1995; Li et al., 1999b) (Figs. 7–9). Considering also the availability of archived 10-day NDVI composites covering Canada, NDVI was chosen for this study. For the analysis of 1995 burns, we used ABC3/NDVI composites from 1–10 September 1994 and 11–20 September 1995. The 1995 composite was selected to include almost the entire fire season while avoiding NDVI decreases due to snow cover and vegetation senescence. The 1–10 September 1994 composite was the final one produced for 1994 due to the failure of the AVHRR sensor aboard NOAA-11. For analysis of 1996 burns we used 11–20 September composites from 1995 and 1996.

A forest mask was developed from a Canada land cover classification produced at Manitoba Remote Sensing Centre using AVHRR imagery (Pokrant, 1991). The classification comprises 10 broad covered types, including four forest types (mixed-wood, deciduous, coniferous, and transitional).

Ground-Truth Data

HANDS 1995 results were compared against data from the National Forestry Database Program (NFD) established by the Canadian Forest Service (http://nfdp.ccfm.org/frames2_e.htm). NFD forest fire statistics are compiled from provincial, territorial, and federal fire management agencies. They include annual forest burned area within each province and territory (for brevity, provinces and territories hereafter are referred to as provinces). Official NFD burned area statistics are not yet published for 1996. For comparison, we therefore used preliminary statistics contained in the 1996 Canada Fire Report produced by the Canadian Interagency Forest Fire Centre.

In addition to calculating burned area, most provinces create GIS surveys of burn boundaries derived from airborne mapping and/or visual interpretation of high-resolution imagery such as Landsat TM. We obtained 1995 burn polygons for five Canadian provinces that had relatively extensive burning (Northwest Territories, Alberta, Saskatchewan, Ontario, and Quebec) and 1996 burn polygons for Quebec. With some exceptions, the surveys do not depict small, unburned islands within burns. The burn polygons were converted to Lambert conformal conic projection, then rasterized to a 500 m resolution grid so that they could be compared against

burns mapped using the HANDS algorithm. Together, the statistical and GIS databases permit a rigorous evaluation of the algorithm.

HANDS ALGORITHM

The HANDS algorithm was developed to combine the strengths of hotspot detection and NDVI differencing for burned area mapping. The aim was to merge the techniques synergistically, allowing each to compensate for deficiencies inherent in the other. The general strategy is to first confirm hotspot pixels using an NDVI difference image. Confirmed hotspots are then used to derive coarse, regional-level NDVI difference thresholds, followed by more restrictive local thresholds. The local thresholds are derived for individual burn patches, which are isolated using GIS clumping techniques. The analyst thus does not need to specify region-specific thresholds, since these are derived from the input data sets. The principal result of the algorithm is to identify burned pixels within scars that were not originally detected as hotspots.

The processing chain, presented below and in Figure 1, is fully automated using a GIS macro. The analyst needs only to prepare the hotspot and vegetation index input data sets described in the previous section. Figure 2 illustrates the key algorithm steps within a region that was subject to several large burns in 1995.

Processing Chain

Step 1. Normalize NDVI composites.

Normalize the postfire NDVI composite to the prefire NDVI composite. This is accomplished by computing the average NDVI for both composites and shifting postfire NDVI values so that the averages are the same [Eq. (2)]. Hotspot pixels are excluded from this calculation. In addition, a land cover classification may be used to isolate a particular vegetation type (e.g., forest) and reduce potential image noise (e.g., from water bodies). When the algorithm is applied over large areas, the NDVI is normalized separately within large, contiguous blocks (e.g., 200×200 km) to account for region-specific NDVI variation:

$$N_{norm(i,j,t)} = N_{(i,j,t)} - [N_{mean(t,b)} - N_{mean(t-1,b)}] \quad (2)$$

where N_{norm} =NDVI normalized composite value, i,j =pixel number, t =year for which hotspots are available, N =NDVI composite value, N_{mean} =mean NDVI composite value, and b =the large block (e.g., 200×200 km) containing pixel $_{i,j}$.

Step 1 compensates for any systematic NDVI variation unrelated to fire. This variation may be associated with seasonal or interannual variation in vegetation phenology, depending on the interval used between composites (Kasischke and French, 1997).

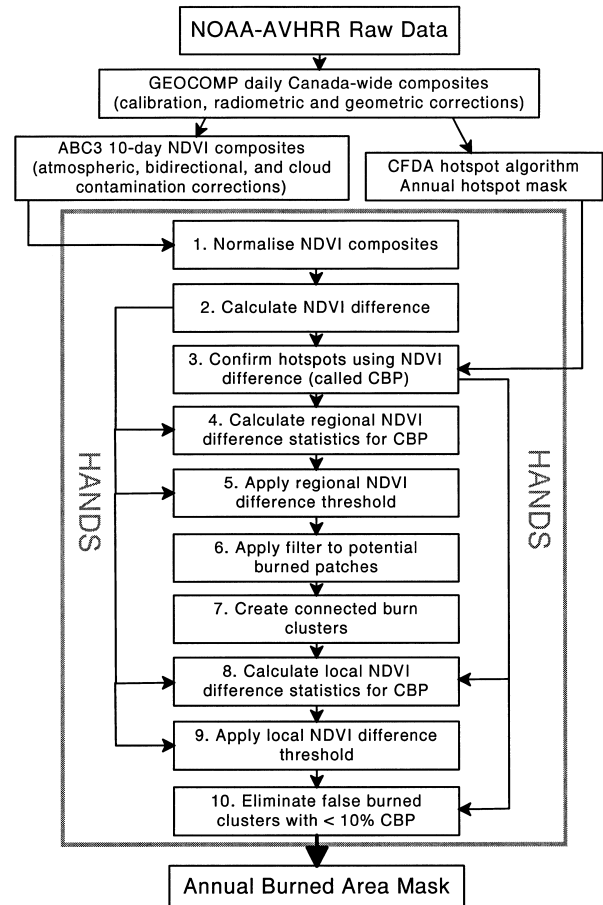


Figure 1. Flowchart showing input data required by HANDS and HANDS processing steps. Arrows represent the flow of input data to each step. Confirmed burn pixels are denoted as CBP.

Step 2. Calculate NDVI difference.

Subtract the prefire composite from the normalised postfire composite. Burned pixels are expected to have a negative value in the resulting NDVI difference image (Fig. 2a) [Eq. (3)]:

$$N_{diff(i,j)} = N_{norm(i,j,t)} - N_{(i,j,t-1)}, \quad (3)$$

where N_{diff} =NDVI difference image.

Step 3. Confirm hotspots using NDVI difference.

Designate hotspot pixels that have an accompanying NDVI decrease as “confirmed burned pixels (CBP)” (Fig. 2b). It is assumed that if a hotspot pixel did not have an NDVI decrease, it was either a falsely detected fire or a small fire causing insignificant vegetation damage at a 1 km² scale. Note that while this assumption is valid for boreal forest, it may not be applicable to environments where NDVI recovers rapidly after burning or where subpixel fires dominate. For 1995, 87% of hotspots pixels detected across Canada are designated as CBP. These CBP are carried forward to the final burned area product in Step 10.

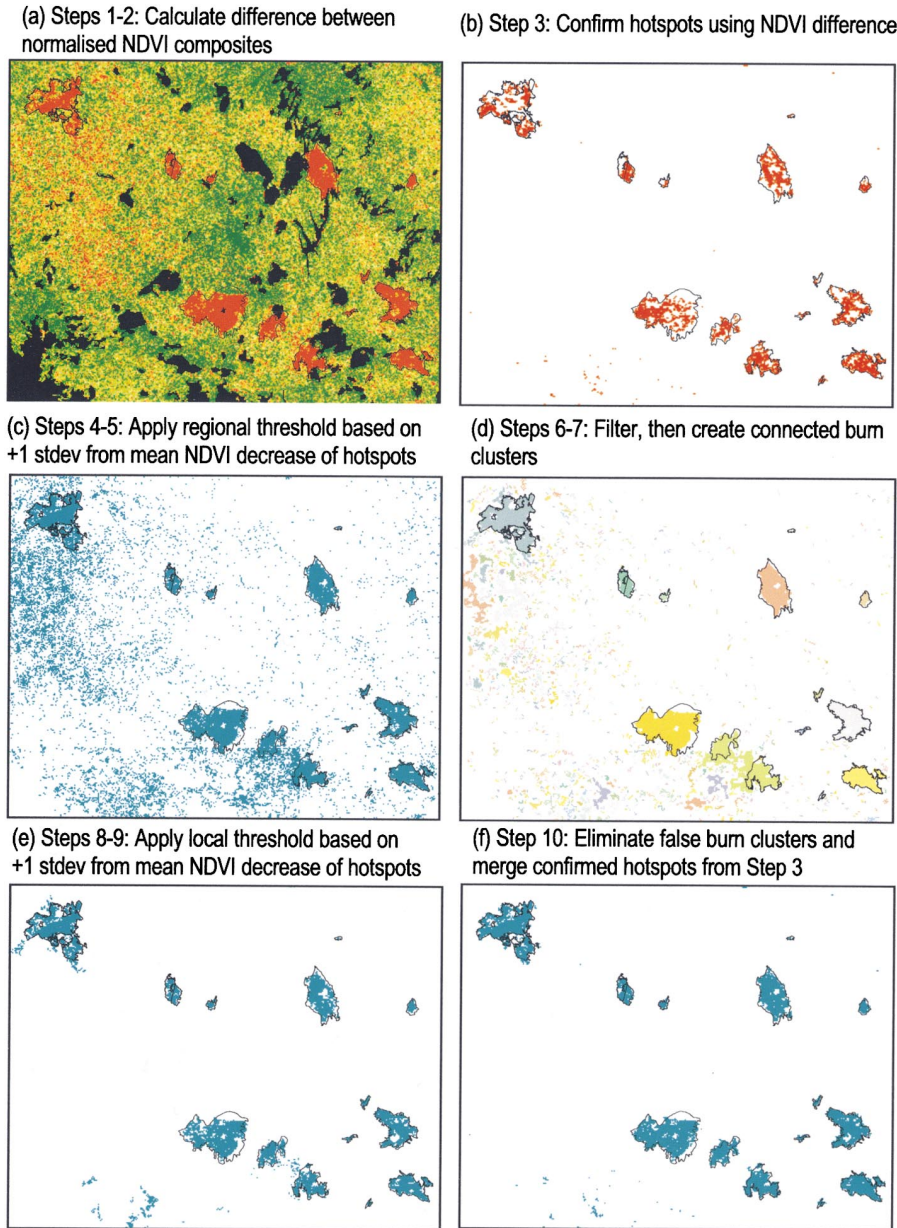


Figure 2. Key processing steps for the HANDS burn mapping algorithm. The color palette in a) ranges from red (large NDVI decrease) to orange (small NDVI decrease) to light green (little NDVI change) to dark green (NDVI increase) with lakes in black. The region shown is a 300 km by 380 km area that was subject to several large burns in 1995.

Step 4. Calculate regional NDVI difference statistics.

Calculate the mean and standard deviation (stdev) of the NDVI difference for all CBP. This is calculated separately within each regional block in the case of a large-scale application [Eqs. (4) and (5)]:

$$N_{\text{mean-diff(CBP},b)} = \text{mean}[N_{\text{diff(CBP},b)}], \quad (4)$$

$$N_{\text{stdev-diff(CBP},b)} = \text{stdev}[N_{\text{diff(CBP},b)}]. \quad (5)$$

where CBP=confirmed burn pixels.

Step 5. Apply a regional NDVI difference threshold.

For each block, select pixels that have an NDVI decrease greater than +1 stdev from the mean NDVI decrease of CBP. This is depicted in Figure 3 and in Eq. (6) below:

$$N_{\text{diff}(i,j)} < N_{\text{mean-diff(CBP},b)} + N_{\text{stdev-diff(CBP},b)}. \quad (6)$$

The block stdev provides a first-pass, regional threshold to isolate patches of potential burned pixels that were not identified as hotspots. These patches are then individually refined in Steps 6–10. The threshold adapts to the degree of fire damage (i.e., NDVI decrease) that is characteristic to the regional assemblage of tree or plant species. For example, in Canada we observed that conifer forest burned in 1995 had an average 12% NDVI decrease, while deciduous forest had a 6% NDVI decrease.

Since the threshold is normally calculated from a large sample of CBP, it is liberal, and includes many nonburned pixels in addition to almost all real burned pixels. Other thresholds were examined (i.e., +2, -1, and -2 stdev, mean) but were found to be too liberal (+2 stdev) or too conservative (mean, -1 and -2 stdev).

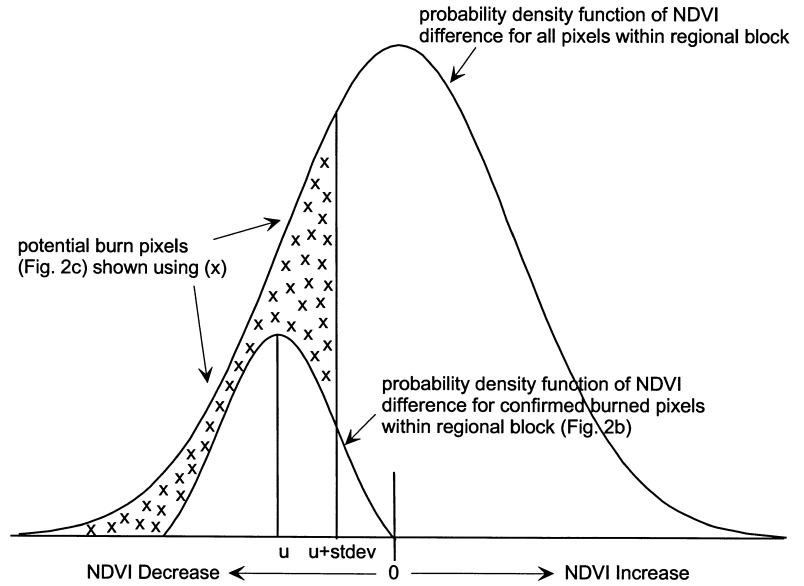


Figure 3. Illustration of HANDS Step 5, in which pixels are selected from each regional block that have an NDVI decrease greater than +1 standard deviation (stdev) from the mean NDVI decrease of confirmed burned pixels. These pixels, shown using “x,” are considered to be potential burn pixels that were not identified as hotspots.

The +1 stdev threshold was found reliable for a wide range of burns across Canada. This step yields Figure 2c.

Step 6. Apply a filter to potential burned patches.

The potential burned pixels from Step 5 are filtered so that each pixel assumes the modal (most commonly occurring) value within its 3 by 3 pixel window. To be retained, a potential burned pixel must thus be surrounded by at least four other potential burned pixels within its eight-cell neighborhood. This step results in smoothing burned patch boundaries and in separating patches from the surrounding background noise (Figs. 2c and 2d). Since a modal filter may substantially alter or eliminate small burned patches, a separate filter is applied if the largest circle that fits entirely inside a patch has a diameter less than 3 pixels (Fig. 4a). In these cases, only single pixels are eliminated in order to reduce noise resulting from the NDVI differencing. The combined result of both filters is illustrated in Figure 4b.

Step 7. Create connected burned clusters.

Group together interconnected burned pixels from Step 6, and assign each resulting cluster a unique code.

Burned pixels are considered connected if they join either diagonally or crosswise. Clusters are shown using separate colors in Figure 2d.

Step 8. Calculate local NDVI difference statistics.

Calculate the mean [Eq. (7) and stdev [Eq. (8)] of the NDVI difference for CBP within each burned cluster created in Step 7:

$$N_{\text{mean-diff(CBP},c)} = \text{mean}[N_{\text{diff(CBP},c)}], \quad (7)$$

$$N_{\text{stdev-diff(CBP},c)} = \text{stdev}[N_{\text{diff(CBP},c)}], \quad (8)$$

where c =single cluster composed of interconnected burned pixels.

Step 9. Apply a local NDVI difference threshold.

Retain pixels within each burned cluster with an NDVI decrease greater than +1 stdev from the mean NDVI decrease of CBP calculated in Step 8 (Fig. 2e):

$$N_{\text{diff}(i,j)} < N_{\text{mean-diff(CBP},c)} + N_{\text{stdev-diff(CBP},c)}. \quad (9)$$

Step 9 is analogous to Step 5, but with the cluster stdev providing a more restrictive, local threshold that adapts

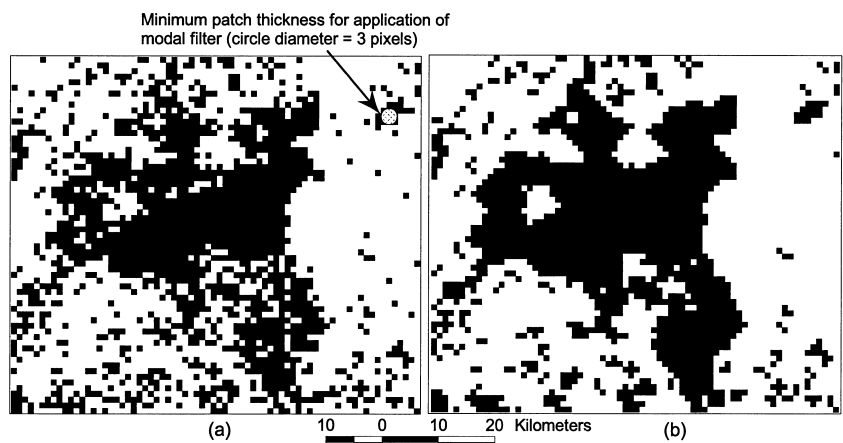


Figure 4. Potential burned pixels separated by applying a regional NDVI difference threshold (HANDS Step 5) are shown in a) for the upper-left area of Figure 2. In Step 6, a filter is applied such that each pixel assumes the modal (most commonly occurring) value within its 3 by 3 pixel window. If a burn patch is small (i.e., the largest circle that fits entirely inside it has a diameter less than three pixels), it is left unchanged and only single pixels are removed. The combined effect of both filters is shown in b).

to the type of vegetation and severity of damage within individual burns. It can also account for the timing of fires, and the subsequent period available for vegetation regeneration leading up to the postfire NDVI composite. Note that clusters containing no CBP are completely removed in this step.

Step 10. Eliminate false burned clusters.

Similar to Step 7, create connected burned clusters using pixels from Step 9 and assign each a unique code. Eliminate any cluster that contains less than 10% CBP, since it is assumed that such clusters represent noise in the NDVI difference image and not real burns (Fig. 2f). This threshold was derived by examining the proportion of hotspots detected within polygons from the 1995 provincial burn surveys. In polygons where at least one CBP was detected, the proportion of CBP was greater than 10% in 98% (191/194) of the cases. A threshold smaller than 10% is able to recover the eliminated clusters that are real burns, but this occurs at the expense of increasing the commission error.

APPLICATION AND EVALUATION

Wildfires have a dominant influence on Canadian boreal forests, affecting ecological succession, primary productivity, and carbon cycling. About 65% of forest fires in Canada are caused by humans, yet lightning ignition is responsible for 85 percent of the annual burned area, which averages 2.4 million ha (Stocks, 1991). The vast majority (>95%) of burning results from intense crown fires that grow larger than 1000 ha (10 km²), making coarse resolution satellite imagery particularly well suited to boreal fire scar mapping.

In 1995, forest fires in Canada were particularly destructive. Fire consumed 7,081,940 ha of forest, making it the second most severe year on record. By contrast, preliminary burn area statistics indicate that, in 1996, fire affected only 1,877,913 ha of forest. To evaluate the burned area mapping algorithm, we applied it across Canada for the 1995 and 1996 fire seasons using the data sets described previously. For comparison, we also calculated 1995 burned area using the NDVI differencing method described in Li et al. (1999b). Briefly, this method involved computing the NDVI difference for a spring pair (21–31 May 1995 and 1996) and fall pair (1–10 September 1994 and 11–20 September 1995) of composites. A pixel was considered burned if it had an NDVI decrease larger than 9% in both pairs and was classified as forest.

Comparison to 1995 Burned Area Statistics and Surveys

Table 1 shows 1995 provincial and national burned area derived using the three satellite-based techniques (CFDA hotspot algorithm, NDVI differencing, and HANDS).

Also included are official NFDP statistics and burned area calculated from the provincial burn polygons. As noted previously, hotspot detection generally underestimates burned area due to low satellite revisit frequency and obscuring by cloud and smoke. Hotspots covered only 69% of the total NFDP 1995 burned area. However, in the five provinces with smallest burned area [British Columbia (BC), Nova Scotia, New Brunswick, Newfoundland, and Prince Edward Island (PEI)], the technique over-represented burning. In Atlantic provinces (Nova Scotia, New Brunswick, Newfoundland, and PEI), this was probably due to the predominance of sub-pixel fires. Burns smaller than 1 km² accounted for 76% of the 1995 burned area in these provinces, compared to only 0.4% for the rest of Canada.

By contrast, NDVI differencing overestimated 1995 burned area in Canada by 39%. This is attributable to various sources of NDVI noise described previously, in addition to real NDVI decreases unrelated to fire. The estimation bias is not constant among provinces, with burned area being significantly underpredicted in Saskatchewan, and overpredicted in Alberta, Yukon, BC and Newfoundland. In some provinces (Ontario, Manitoba, Quebec) NDVI differencing estimates were reasonably close to NFDP figures. However, in these cases, provincial burn surveys indicate that NDVI commission errors arising from noise compensated for NDVI omission errors within actual burns.

When the hotspot and NDVI methods are combined (i.e., HANDS), the accuracy of burned area estimates increased. Canada-wide burned area was calculated to be 6.8 million ha, compared to 7.1 million ha from NFDP. According to the Canada land cover classification (Pokrant, 1991), coniferous forest was the predominant forest type burned (66%), followed by transitional forest (21%), mixed-wood forest (11%), and deciduous forest (2%). The provincial estimates from HANDS were consistently close to NFDP values, with the exception of Northwest Territories (NWT) and BC. The cause of the discrepancy for NWT is not clear, as mapped burn boundaries match up very well with the NWT burn survey (also note the similar areas in Table 1). The overprediction for BC is also difficult to reconcile, especially without the benefit of independent ground data. One possibility is that snow reflection and AVHRR noise caused by abrupt changes in relief may have led to apparent hotspots and NDVI decrease. Note that the hotspot and NDVI differencing techniques both produced large overestimates for this province.

A more rigorous evaluation of the mapping algorithm can be performed using polygon burn surveys that were available from five provinces. Figure 5 shows the relationship between the area of each provincial polygon and the corresponding HANDS burned area. Data are presented on a logarithmic scale so that the distribution of values can be clearly observed. In cases where there were more than one HANDS burn inside a polygon, or

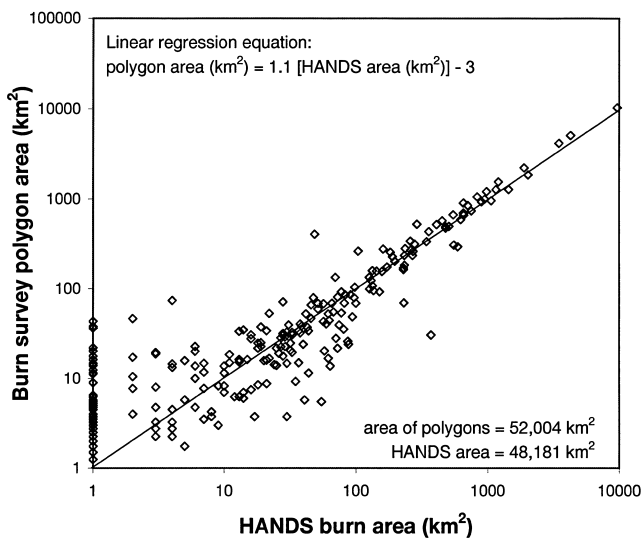
Table 1. Comparison of Burned Area (ha) for 1995 from Various Mapping Sources

Province	CFDA Hotspots	NDVI Differencing	HANDS Algorithm	CFS NFDP	Provincial Fire Polygons
Northwest Territories	1,677,600	2,024,500	2,143,300	2,827,400	2,165,338
Saskatchewan	1,040,000	843,400	1,486,900	1,386,929	1,377,769
Manitoba	674,100	768,900	1,029,700	889,248	N/A
Quebec	637,900	659,500	801,800	708,100 ^a	758,037
Ontario	363,000	626,100	715,100	612,437	526,326
Alberta	241,100	568,00	315,000	342,610	308,928
Yukon	174,100	503,700	225,800	258,403	N/A
British Columbia	82,700	3,636,300	115,000	48,080	N/A
Nova Scotia	2300	1000	1600	405	N/A
New Brunswick	2100	2200	1100	416	N/A
Newfoundland	4300	154,000	1400	794	N/A
Prince Edward Island	200	0	700	36	N/A
Parks Canada	N/A	N/A	N/A	7082	N/A
Total	4,890,000	9,811,000	6,837,400	7,081,940 ^a	N/A

^a Quebec burn area includes modified fire response zones not shown in official NFDP figures.

vice versa, they were merged and their areas summed. The overall association is very close ($r^2=0.99$, $p<0.005$, $n=276$, nontransformed values), but becomes weaker and nonlinear for burns smaller than about 10 km². HANDS did not map 30% (82/276) of the provincial polygons, which lie on the y -axis in Figure 5. The hotspot algorithm did not detect any active fires within these polygons, representing an inherent constraint to the HANDS technique. Nevertheless, the majority of missed burns (70/82) was smaller than 10 km², which is consistent with the findings of Pereira et al. (1999) using AVHRR in a Mediterranean environment. These missed burns accounted for less than 1% of the total area of polygons, while, more generally, burns smaller than 10

Figure 5. The relationship between the area of each provincial burn polygon ($n=276$) and the corresponding burned area computed by HANDS. Data are presented on a logarithmic scale, with a line showing 1:1 agreement. Samples on the y -axis represent polygons that contained no hotspots.



km² were responsible for only 3% of total forest burned area in Canada from 1990–1995.

Figure 6a–e shows burn polygon boundaries for major burned areas within each province. Burned forest pixels identified using the HANDS algorithm are shown in grey. For the majority of burns, there is good agreement between the boundaries from the two mapping sources. The most notable differences occur within smaller burns. Some small burns were contaminated by background noise resulting from the NDVI differencing (Fig. 6c), while others were mostly or entirely missed (shown in Figs. 6c and 6e inside squares). As indicated above, burns that were completely missed had no active fires detected within them.

Several HANDS burns are not shown in the provincial surveys. To determine if the larger of these (>50 km²) were errors of commission or real burns that went undetected, we looked at several sources of evidence. These included: 1) prefire and post-fire NDVI composites and single scenes to identify uniform patches of NDVI decrease; 2) the proportion of hotspots detected over each such burn; 3) a comparison of scars with those from 1994, to determine if the burns occurred in 1994; and 4) single AVHRR scenes to detect visible smoke plumes emanating from the burns. Within the five provinces for which surveys were available, a total of 22 burns larger than 50 km² were identified by HANDS that do not appear on the surveys. Based on the above lines of evidence, 15 were real burns comprising an area of 2562 km². These include all the burns outlined by circles in Figures 6c and 6d. The remaining seven burns are likely falsely mapped burns, covering 1373 km². Four of the false burns occur at the location of 1994 burns (three of which are outlined by triangles in Fig. 6e), while three are attributable to other sources of noise. In cases where the algorithm erroneously identified burns, there are concurrent failure in the hotspot and NDVI

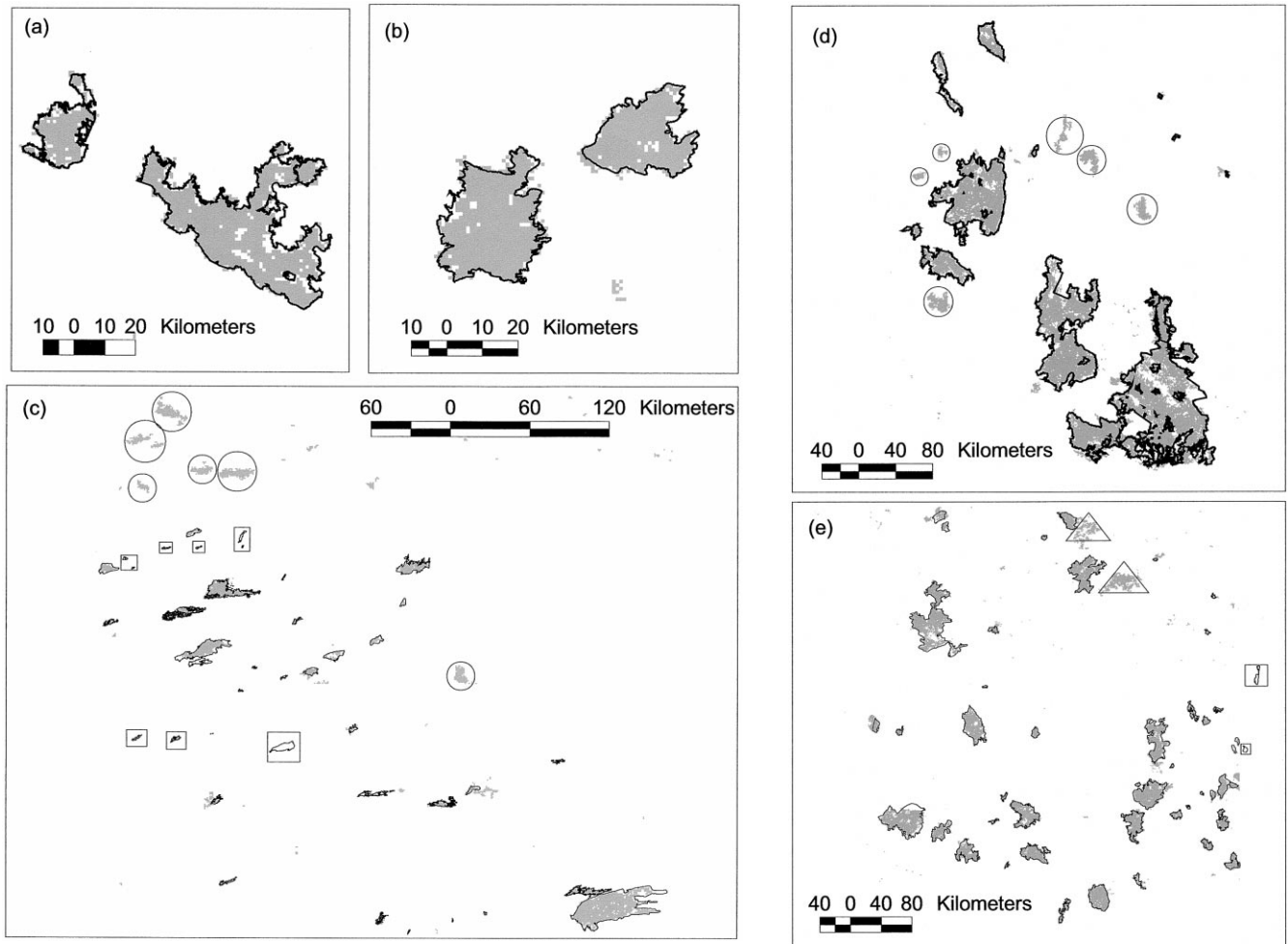


Figure 6. Major burned areas within the five provinces for which detailed burn surveys were available. Survey polygons are outlined in black, while HANDS burn pixels are shown in grey. The square outlines in c) and e) identify burn polygons that were not identified by HANDS (omission errors). The triangle outlines in e) delineate burns that were falsely mapped by the algorithm (commission errors). Several real burns identified by HANDS but not included in the surveys are outlined by circles in c) and d).

differencing methods. In particular, scattered hotspots were detected in several 1994 burns due to their high surface temperatures and large Channel 3 response. In addition, these 1994 burns are often more discernible in the September 1995 NOAA-14 NDVI composite compared to the September 1994 NOAA-11 NDVI composite, producing an apparent NDVI decrease. The 1994 composite is relatively noisy, which may be related to the decline of the AVHRR sensor aboard NOAA-11 prior to its failure in late 1994.

In some individual burns, boundaries derived using HANDS differed significantly from those indicated in the provincial surveys. For example, Figure 7a shows polygon boundaries for three large burns. Pixels corresponding to HANDS scars are displayed in grey, while pixels representing both HANDS scars and confirmed hotspots are displayed in black. In the largest burn, the boundaries coincided only over a small area, while in the

burn to the south-east, the survey polygon was much smaller. Figure 7b shows the 11–19 September 1995 NDVI composite for the area. By comparison to an earlier 21–30 May 1995 composite (Fig. 7c), pixels corresponding to HANDS scars are observed to have a clear NDVI decrease. If the distribution of hotspots is also considered, it appears that in these cases, the mapping algorithm provided a more accurate representation of the burned area.

Figures 8a–c and 9a–c show a similar series of images for burns in two other provinces. In Figure 8, the survey polygon extends beyond both the HANDS scar and area of NDVI decrease in several locations. One reason for this difference may be that the outer region of the aerial survey covers ground fires that did not spread to the tree crowns. Smouldering ground fires may be neither hot enough to create a strong signal in the mid-infrared channel nor cause an AVHRR-NDVI decrease

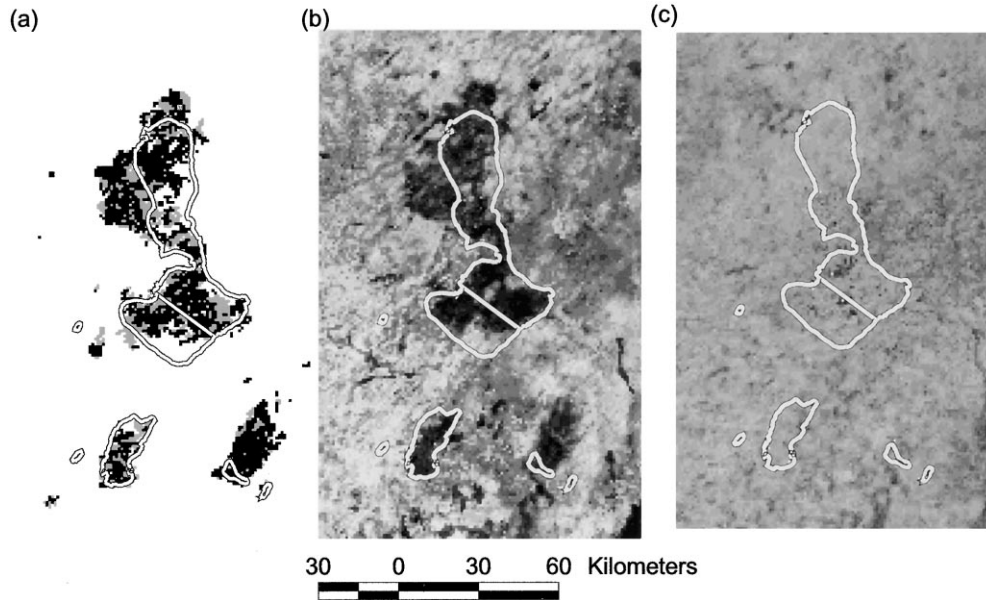


Figure 7. Example in which survey polygon boundaries differed significantly from HANDS results. a) Pixels corresponding to HANDS scars are shown in grey, while pixels representing HANDS scars and confirmed hotspots are shown in black. The boundary from the provincial burn survey is also shown. b) Postfire (11–20 September 1995) NDVI composite with survey boundary overlaid. Smaller NDVI values appear as darker shades of grey. c) (Prefire 21–30 May 1995) NDVI composite with survey boundary overlaid.

since the above canopy is not damaged. In Figure 9a, HANDS identified several apparently unburned areas within a large burn polygon. The post- and prefire NDVI composites (Figs. 9b and 9c) would also suggest that most of these islands were not burned. However, it is possible again that these may be areas subjected to ground fires that caused minimal canopy damage. It seems that the mapping algorithm, at least when used in conjunction with AVHRR, is best suited for mapping intense burns where there has been appreciable scarring of tree crowns.

Comparison to 1996 Burned Area Statistics and Survey

Provincial burn surveys from 1995 were used to aid the development of the HANDS algorithm. To provide a second, independent validation of the algorithm, we applied it to the 1996 fire season. The preliminary nature of the 1996 burned area statistics and paucity of 1996 provincial burn surveys precluded a detailed analysis of the results. However, at a national level, burned area computed using HANDS (2,037,500 ha) compared favorably with burned area (1,877,913 ha) estimated as of 31 December 1996 using conventional methods (Canada Fire Report for 1996, Canadian Interagency Forest Fire Centre, <http://www.cifcc.ca/>). Moreover, we obtained a 1996 GIS burn survey for Quebec, which had the largest burned area of all provinces. Figure 10 shows survey polygons and HANDS scars for the major burned area in Quebec. As in the 1995 comparisons, the mapping al-

gorithm output closely corresponded to the polygon survey boundaries. HANDS missed a few small burns (inside squares), but did identify a few real burns not shown in the survey (inside circles).

Application Using a Global Fire Detection Algorithm

A desirable characteristic of a satellite burn mapping technique is that it be adaptable to different input data sets. To assess this ability of HANDS, we used the IGBP contextual fire detection algorithm (IGBP-DIS, 1997) to provide hotspot input data. The IGBP algorithm, based on Flasse and Ceccato (1996), was developed for global application with NOAA-11/AVHRR imagery and is currently applied to NOAA-14 data for global fire monitoring as part of the World Fire Web. Li et al. (1999b) applied the IGBP algorithm to 1995 NOAA-14/AVHRR imagery over two provinces to assess its performance for Canadian boreal forest. The algorithm detected a similar proportion (48%) of the conventionally mapped burned area as the CFDA (60%). However, it also was prone to detecting false fires at the location of 1994 burns. This is illustrated in Figures 11a and 11b for major burned area within each province. Hotspots derived for 1995 using the IGBP algorithm are shown in grey and provincial survey polygons are outlined in black.

Results from inputting IGBP hotspots to the mapping algorithm are shown in Figure 11c and 11d. In all burn polygons, the ability of HANDS to identify burned

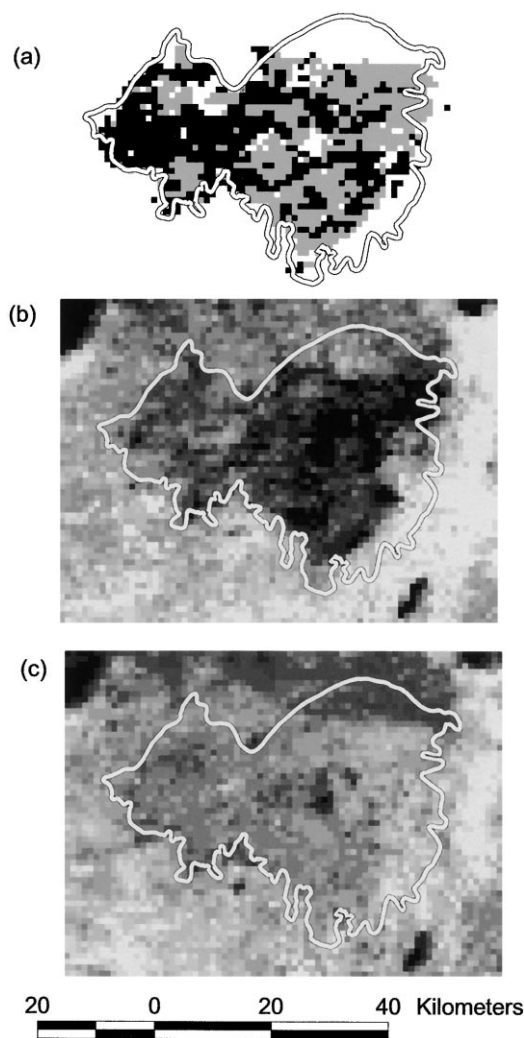


Figure 8. Example in which the survey boundary extended beyond the burned area mapped by HANDS. a) Pixels corresponding to HANDS scars are shown in grey, while pixels representing HANDS scars and confirmed hotspots are shown in black. The boundary from the provincial burn survey is also shown. b) Postfire (11–20 September 1995) NDVI composite with survey boundary overlaid. Smaller NDVI values appear as darker shades of grey. c) Prefire (21–30 May 1995) NDVI composite with survey boundary overlaid. The white patch at the centre of the burn in a) is a lake.

areas that were not detected as hotspots was comparable to that when CFDA hotspots were used (Figs. 6d and 6e). By combining the NDVI differencing and hotspot detection strategies, the technique was also able to eliminate many falsely detected IGBP fires. Yet, there still remain several large burns mapped at the location of 1994 fires. As noted previously, these false scars are attributable to the IGBP algorithm detecting hotspots in 1994 burns and to the fact that many 1994 burns are more visible in the 1995 NDVI composite than in the 1994 NDVI composite.

SUMMARY AND CONCLUSIONS

This article presents HANDS, a new satellite-based algorithm for boreal burned area mapping. HANDS synergistically combines two methods commonly used for burn assessment: hotspot detection and multitemporal NDVI differencing. Hotspots are used to dynamically train an NDVI difference threshold for separating scars. NDVI differencing is used to remove falsely detected hotspots and to fill in patches within individual burns that were not detected as hotspots. The overall result is a close approximation to actual burn boundaries, within the limits of the input data. Using the technique, burn mapping may be performed in a consistent and automated manner over large regions.

To evaluate the method, we applied it to mapping forest fire burns occurring across Canada in 1995 and 1996. National burned area was calculated to be 6.8 million ha in 1995 and 2.0 million ha in 1996, comparing favorably to Canada Forest Service estimates of 7.1 and 1.9 million ha, respectively. At local scales, the HANDS burns also corresponded well to provincial burned area statistics and to individual burn polygons derived from aerial surveys. In several cases, HANDS was able to identify burns that were not shown in the surveys. The algorithm did cause a few large burns ($>50 \text{ km}^2$) to be incorrectly identified for 1995. These were attributed to the poorer quality of the 1994 NDVI composite compared to the 1995 composite, and to the fact that several 1995 hotspots were detected inside 1994 burns.

When used in conjunction with AVHRR imagery, HANDS seems best suited to mapping large ($>10 \text{ km}^2$), intense fires, which are characteristic for the boreal biome. The coarse footprint of AVHRR pixels ($1.2\text{--}15 \text{ km}^2$) would hamper application of the method to tropical forest, where fires are often smaller than 1 km^2 (Setzer and Pereira, 1991). However, in principle, the technique should be adaptable to other biomes and environments provided the following conditions are met:

1. Hotspots are detected over at least a small portion (e.g., $>10\%$) of each burn. This condition can be normally satisfied in boreal forest using single sensor (e.g., NOAA-14/AVHRR) hotspot detection. In other environments where small burn patches may be responsible for a significant fraction of the burned area, hotspot detection from multiple sensors (e.g., NOAA-14/15, MODIS, GOES-8, ATSR-2) would likely be required.
2. Burned vegetation is spectrally separable from unburned vegetation using available satellite bands and/or band combinations. For example, AVHRR indices based on the NIR/MIR spectral domain (Barbosa et al., 1999; Pereira, 1999) or a short-wave infrared (SWIR) channel (Eva and Lambin, 1998) are preferable to NDVI for detecting burns in Mediterranean and African ecosystems.

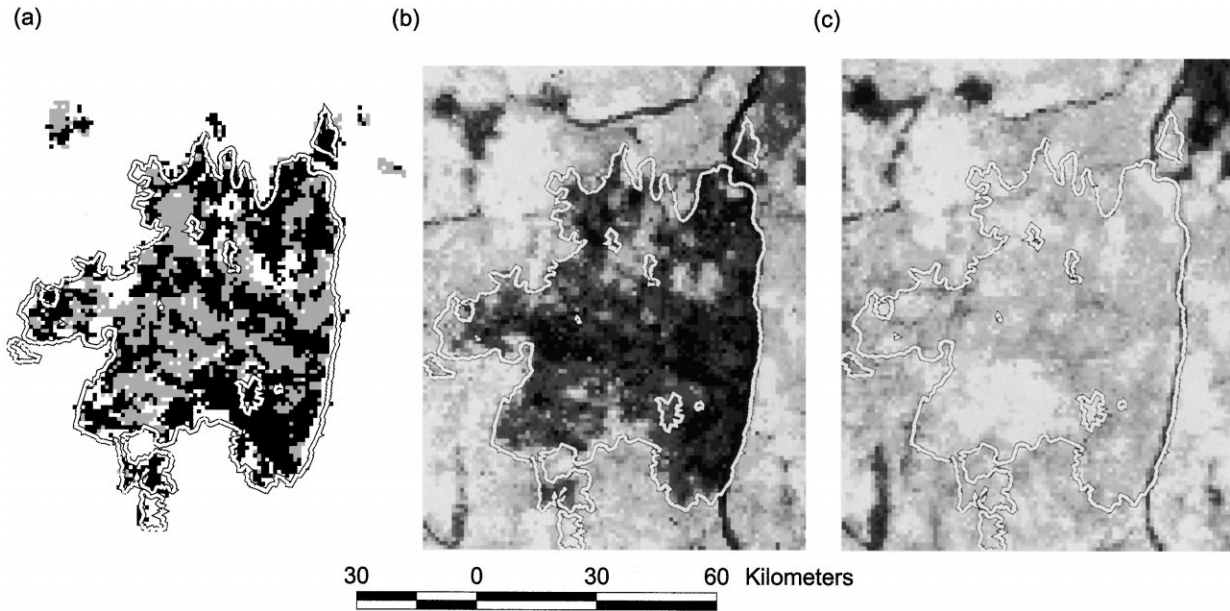


Figure 9. Example in which the HANDS algorithm appears to identify unburned islands within a large burn. a) Pixels corresponding to HANDS scars are shown in grey, while pixels representing HANDS scars and confirmed hotspots are shown in black. The boundary from the provincial burn survey is also shown. b) Postfire (11–20 September 1995) NDVI composite with survey boundary overlaid. Smaller NDVI values appear as darker shades of grey. c) Prefire (21–30 May 1995) NDVI composite with survey boundary overlaid.

3. Satellite imagery is available for multitemporal differencing that has a spatial resolution smaller than the size of burns typical for the environment.
4. Multitemporal differencing can be performed over a time interval shorter than the duration of the spectral response to burning. For example, a 15-day interval or shorter may be necessary to map burned tree savannah, where the burn signal tends to attenuate rapidly (Barbosa et al., 1998).

Recently launched or planned space-borne sensors should allow these requirements to be met for a larger

range of environments. The SPOT VEGETATION instrument, launched in March 1998, includes a 1.1-km resolution SWIR channel (1.65 μm) that initial analysis has shown to exhibit increased reflectance for several years in burned boreal forest. This is consistent with earlier findings using the Landsat Thematic Mapper (Ahern and Archibald, 1986). In addition, VEGETATION has superior radiometric and geometric characteristics compared to AVHRR, with a nearly constant across-track resolution. A 1998 Canada-wide burned area mask is currently being validated that was produced by synergistically com-

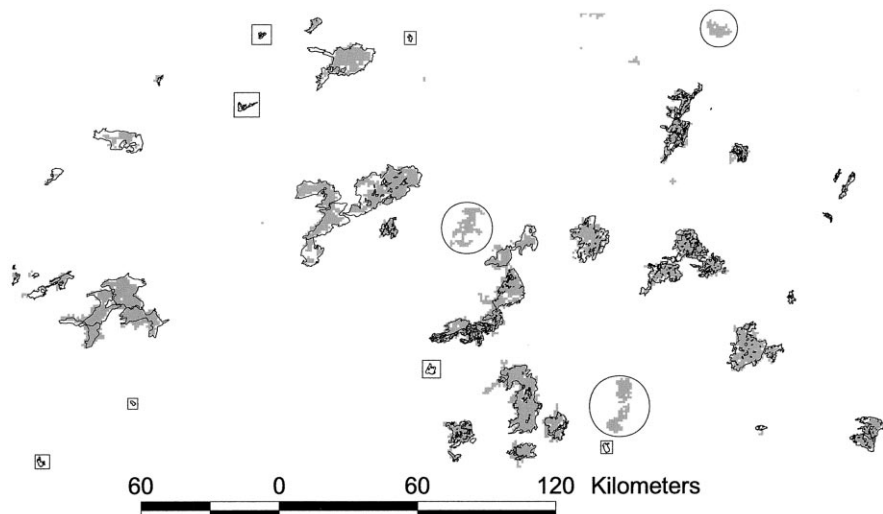


Figure 10. Major burned area within Quebec for 1996. Provincial burn polygons are outlined in black, while HANDS burn pixels are shown in grey. A few real burns identified by HANDS but not shown in the survey are outlined in circles, while burns missed by HANDS are outlines in squares.

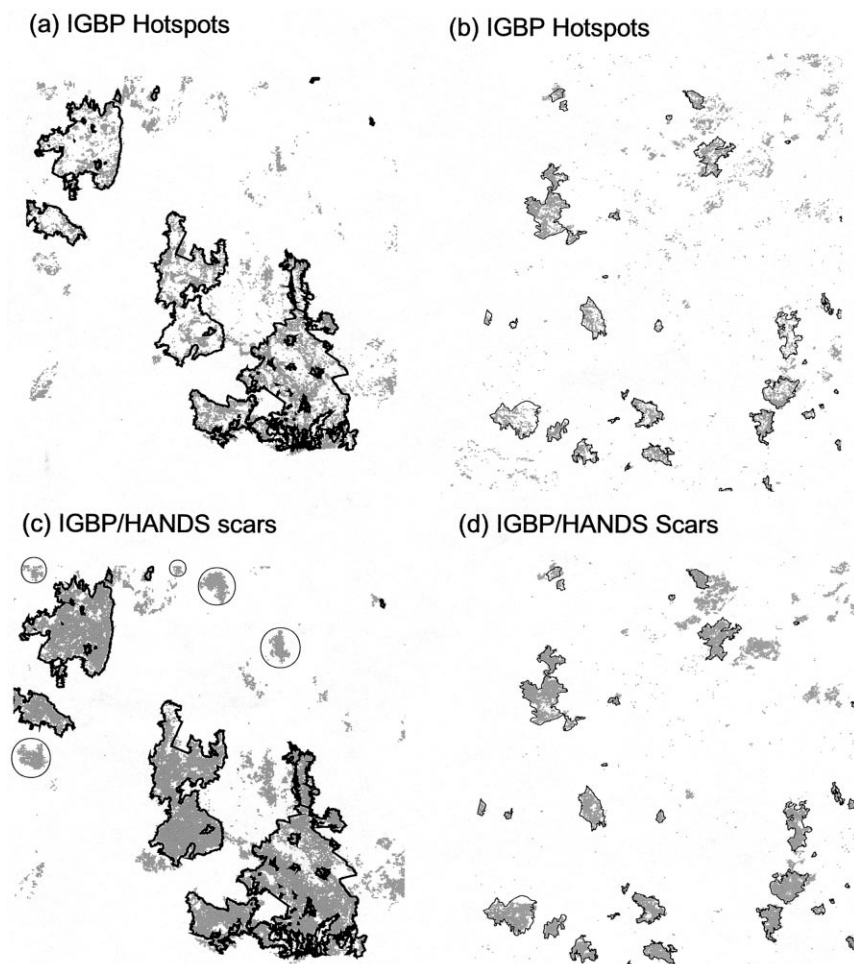


Figure 11. Results from inputting IGBP hotspots (IGBP-DIS, 1997) to the burn mapping algorithm. In a) and b) 1995 IGBP hotspots are shown in grey and provincial survey polygons are outlined in black; c) and d) show burned areas mapped by HANDS using IGBP hotspots as input.

binning annual AVHRR hotspots with multi-temporal differencing of an index $[(NIR - SWIR)/(NIR + SWIR)]$ derived from VEGETATION composites.

The Moderate Resolution Imaging Spectroradiometer (MODIS) is due to be launched in late 1999 aboard NASA's Terra (EOS-AM) satellite. MODIS will contain 1-km resolution channels at $4 \mu m$ and $11 \mu m$ designed specifically for monitoring fire hotspots (Kaufman et al., 1998). Eventually, MODIS sensors aboard EOS-AM and EOS-PM will provide four daily hotspot observations over most of the earth. Standard fire products will be generated and archived that summarize fire occurrence and location over daily, 8-day, and monthly intervals. These products could be synergistically combined with multitemporal analysis of MODIS's 250-m vegetation indices and/or 500-m infrared channels ($1.6 \mu m$, $2.1 \mu m$). This could allow for the first time, accurate global measurement of biomass burning, both for burned area statistics and for local burn boundaries.

We thank John Mason at the Canadian Forest Service Great Lakes Forestry Centre for providing GIS burn surveys; Albert Simard at the Canada Forest Service in Ottawa for helpful dis-

cussion of forest fire statistics; and Frank Ahern at the Canada Centre for Remote Sensing for reviewing the manuscript. Algorithm development and testing would not have been possible without the availability of detailed burn surveys produced by fire agencies from Northwest Territories, Alberta, Saskatchewan, Ontario, and Quebec.

REFERENCES

- Ahern, F. J., and Archibald, P. D. (1986), Thematic Mapper information about Canadian forests: early result from across the country. In Proceedings of the Tenth Canadian Symposium on Remote Sensing, Canadian Aeronautics and Space Institute, Edmonton, Alberta, May 5–6 1986, pp. 683–697.
- Andreae, M. O., Atlas, E., Cachier, H., et al. (1996), Trace gas and aerosol emissions from savanna fires. In *Biomass Burning* (J. S. Levine, Ed.), MIT Press, Cambridge, pp. 278–295.
- Barbosa, P. M., Pereira, J. M. C., and Gregoire, J. M. (1998), Compositing criteria for burned area assessment using multispectral low resolution satellite data. *Remote Sens. Environ.* 65:38–49.
- Barbosa, P. M., Gregoire, J. M., and Pereira, J. M. C. (1999), An algorithm for extracting burned areas from time series

- of AVHRR GAC data applied at a continental scale. *Remote Sens. Environ.* 69:253–263.
- Cahoon, D. R., Stocks, B. J., Levine, J. S., Cofer, W. R., and Pierson, J. M. (1994), Satellite analysis of the severe 1987 forest fires in northern China and southeastern Siberia. *J. Geophys. Res.* 99:18,627–18,638.
- Christensen, N. L. (1993), Fire regimes and ecosystem dynamics. In *Fire in the Environment* (P. J. Crutzen and J. G. Goldammer, Eds.), Wiley, New York, pp. 233–244.
- Canadian Interagency Forest Fire Center (CIFFC) (1995), Canada Fire Report for 1995, North American Forestry Commission Fire Management Study Group 29th Meeting, Merida, Yucatan, Mexico.
- Cihlar, J. (1996), Identification of contaminated pixels in AVHRR composite images for studies of land biosphere. *Remote Sens. Environ.* 56:149–163.
- Cihlar, J., Ly, H., Li, Z., Chen, J., Pokrant, H., and Huang, F. (1997), Multitemporal, multichannel AVHRR data sets for land biosphere studies: artifacts and corrections. *Remote Sens. Environ.* 60:35–57.
- Crutzen, P. J., and Andreae, M. O. (1990), Biomass burning in the tropics: impact on atmospheric chemistry and biogeochemical cycles. *Science* 250:1669–1678.
- Dwyer, E., Gregoire, J.-M., and Malingreau, J.-P. (1998), Global analysis of vegetation fires using satellite images: spatial and temporal dynamics. *Ambio* 27:175–181.
- Eva, H., and Lambin, E. F. (1998), Burnt area mapping in Central Africa using ATSR data. *Int. J. Remote Sens.* 19:3473–3497.
- Fernandez, A., Illera, P., and Casanova, J. L. (1997), Automatic mapping of surfaces affected by forest fires in Spain using AVHRR NDVI composite image data. *Remote Sens. Environ.* 60:153–162.
- Flannigan, M. D., and Vonder Haar, T. H. (1986), Forest fire monitoring using NOAA satellite AVHRR. *Can. J. For. Res.* 16:975–982.
- Flasse, S. P., and Ceccato, P. (1996), A contextual algorithm for AVHRR fire detection. *Int. J. Remote Sens.* 17:419–424.
- Harris, A. J. (1996), Towards automated fire monitoring from space: semi-automated mapping of the January 1994 New South Wales wildfires using AVHRR data. *Int. J. Wild. Fire* 6:107–116.
- International Geosphere Biosphere Programme, Data and Information Systems (IGBP-DIS) (1997), Definition and implementation of a global fire product derived from AVHRR data, IGBP-DIS Working Paper #17, 3rd IGBP-DIS Fire Working Group Meeting Report, Toulouse, France, 13–15 November 1996.
- Justice, C. O., Kendall, J. D., Dowty, P. R., and Scholes, R. J. (1996), Satellite remote sensing of fires during the SAFARI campaign using NOAA advanced very high resolution radiometer data. *J. Geophys. Res.* 101:23,851–23,863.
- Kasischke, E. S., and French, N. H. (1995), Locating and estimating the areal extent of wildfires in Alaskan boreal forests using multiple-season AVHRR NDVI composite data. *Remote Sens. Environ.* 51:263–275.
- Kasischke, E. S., and French, N. H. (1997), Constraints on using AVHRR composite index imagery to study patterns of vegetation cover in boreal forests. *Int. J. Remote Sens.* 18:2403–2426.
- Kasischke, E. S., French, N. H., Harrell, P., Christensen, N. L., Ustin, S. L., and Barry, D. (1993), Monitoring of wildfires in boreal forests using large area AVHRR NDVI composite image data. *Remote Sens. Environ.* 45:61–71.
- Kasischke, E. S., French, N. F., Bourgeau-Chavez, L. L., and Christensen, N. L. (1995), Estimating release of carbon from 1990 and 1991 forest fires in Alaska. *J. Geophys. Res.* 100:2941–2951.
- Kaufman, Y., Tucker, C., and Fung, I. (1990), Remote sensing of biomass burning in the tropics. *J. Geophys. Res.* 95:23,851–23,863.
- Kaufman, Y., Justice, C., Flynn, L. et al. (1998), Potential global fire monitoring from EOS-MODIS. *J. Geophys. Res.* 103:32,215–32,338.
- Kennedy, P. J., Belward, A. S., and Gregoire, J.-M. (1994), An improved approach to fire monitoring in West Africa using AVHRR data. *Int. J. Remote Sens.* 15:2235–2255.
- Levine, J. S., Ed. (1996), *Biomass Burning and Global Change*, MIT Press, Cambridge, MA.
- Li, Z., Cihlar, J., Moreau, L., Huang, F., and Lee, B. (1997), Monitoring fire activities in the boreal ecosystem. *J. Geophys. Res.* 102:29,611–29,624.
- Li, Z., Nadon, S., and Cihlar, J. (1999a), Satellite detection of Canadian boreal forest fires: development and application of the algorithm. *Int. J. Remote Sens.* in press.
- Li, Z., Nadon, S., Stocks, B., and Cihlar, J. (1999b), Satellite detection of Canadian boreal forest fires part I: algorithm validation and comparison. *Int. J. Remote Sens.*, in press.
- Lovejoy, T. E. (1991), Biomass burning and the disappearing tropical rainforest. In *Global Biomass Burning* (J. S. Levine, Ed.), MIT Press, Cambridge, pp. 77–82.
- Martin, M. P., and Chuvieco, E. (1995), Mapping and evaluation of burned land from multitemporal analysis of AVHRR NDVI images. *EARSEL Adv. Remote Sens.* 4:7–13.
- Menaut, J.-C., Abbadie, L., and Vitousek, P. M. (1993), Nutrient and organic matter dynamics in tropical ecosystems. In *Fire in the Environment* (P. J. Crutzen and J. G. Goldammer, Eds.), Wiley, New York, pp. 215–230.
- Pereira, J. M. C. (1999), A comparative evaluation of NOAA/AVHRR vegetation indexes for burned surface detection and mapping. *IEEE Trans. Geosci. Remote Sens.* 37:217–226.
- Pereira, A. C., and Setzer, A. W. (1996), Comparison of fire detection in savannas using AVHRR's Channel 3 and TM images. *Int. J. Remote Sens.* 17:1925–1937.
- Pereira, J. M. C., Sousa, A. M. O., and Sa, A. C. L. (1999), Regional scale burnt area mapping in Southern Europe using NOAA-AVHRR 1km data. In *Remote Sensing of Large Wildfires in the European Mediterranean Basin* (E. Chuvieco, Ed.), Springer-Verlag, Berlin, pp. 139–155.
- Pokrant, H. (1991), Land cover map of Canada derived from AVHRR images, Manitoba Remote Sensing Centre, Winnipeg, Manitoba, Canada.
- Randriambelo, T., Baldy, S., Bessafi, M., Petit, M., and Despinoy, M. (1998), An improved detection and characterization of active fires and smoke plumes in south-eastern Africa and Madagascar. *Int. J. Remote Sens.* 19:2623–2638.
- Robertson, B., Erickson, A., Friedel, J., et al. (1992), GEOCOMP: a NOAA AVHRR geocoding and compositing system. In *Proceedings, ISPRS Conference, Commission 2, International Society for Photogrammetry and Remote Sensing*, Washington, DC, pp. 223–228.

- Robinson, J. M. (1991), Fire from space: global fire evaluation using infrared remote sensing. *Int. J. Remote Sens.* 12:3–24.
- Roy, D. P., Giglio, L., Kendall, J. D., and Justice, C. O. (1999), Multi-temporal active-fire based burn scar detection algorithm. *Int. J. Remote Sens.* 20:1031–1038.
- Running, S. W., Peterson, D. L., Spanner, M. A., and Teuber, K. B. (1986), Remote sensing of coniferous forest leaf area. *Ecology* 67:273–276.
- Setzer, A. W., and Pereira, M. C. (1991), Amazonia biomass burnings in 1987 and an estimate of their tropospheric emissions. *Ambio* 20:19–22.
- Stocks, B. J. (1991), The extent and impact of forest fires in northern circumpolar countries. In *Global Biomass Burning: Atmospheric, Climatic, and Biospheric Implications* (J. S. Levine, Ed.), MIT Press, Cambridge, MA, pp. 197–202.